Supplementary material

1 Zonal integral versus zonal mean

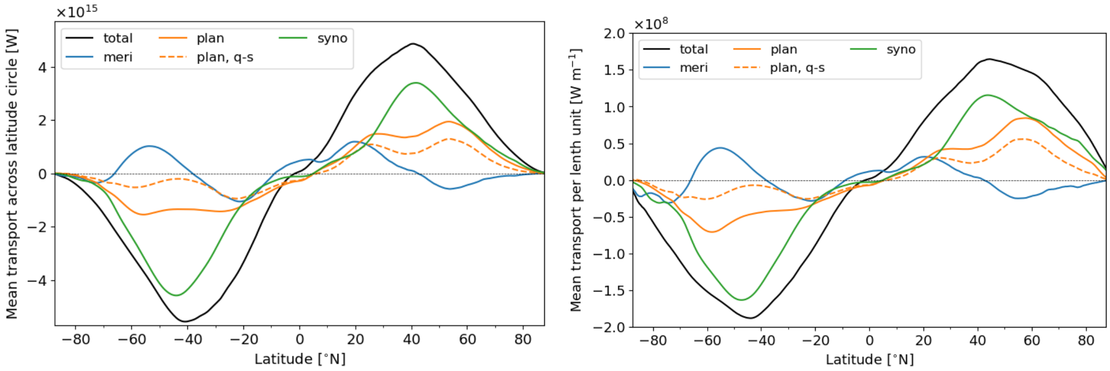

(a) Integral over latitude cycle

(b) Zonal mean

Figure S1: Different perspectives on the separation of the annual-mean energy transport, $\widetilde{vE}$, (black) from ERA5. (a) Depicts the transport across a latitude band in a similar manner as Graversen and Burtu [2016]. (b) Displays the zonal-mean transport providing an average local transport as utilised in this study. In both panels, the meridional overturning circulation is captured by wave 0, whereas planetary and synoptic transport are separated at a wavelength of 8,000 km. For the planetary transport also the quasi-stationary component is displayed.

2 A continuous separation by wavelength

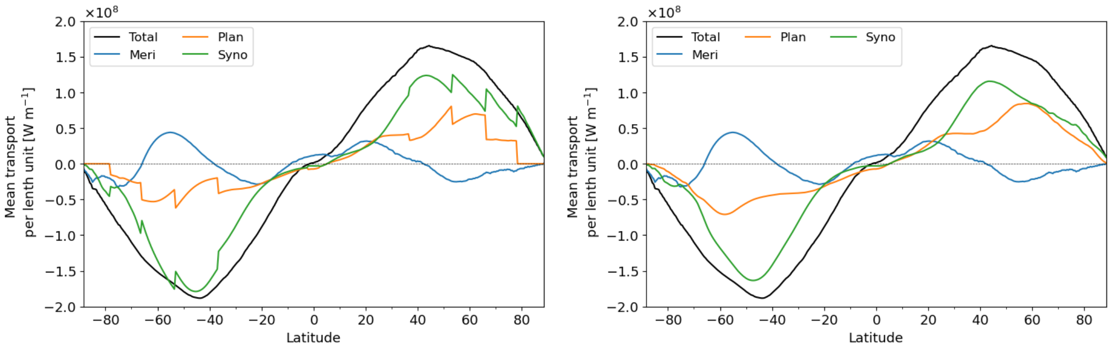

(a) Wavelength strict separation

(b) Wavelength continuous separation

Figure S2: Comparison of a strict and a continuous separation of the annual-mean energy transport, $\widetilde{vE}$, (black) from ERA5 in a similar manner as in Figure S1b. (a) Strict separation, where the separation is such that all waves below the separation number, given by the wavenumber corresponding to a wavelength of 8,000 km at each latitude, are defined as planetary and those larger the separation number as synoptic. (b) Continuous separation according to Equation 9 as applied in the study, where the decimal digit of the separation number is partitioned between the scales.

3 Spectra depicted the scale separation at different latitudes

Figure S3 shows the separation of the meridional energy transport by different waves at different latitudes. It is a different depiction of Figure 2, and we use it to describe the separation into different scales by an example that helps to interprete Equation 9.

For example, at ϕ =40° N, the separation between the planetary scale (s in Eq. 9) and synoptic scale ($s+1$) at the defined wavelength of $\lambda_{syno} = 8000$ km is performed by the separation number, $n_{syno} = \frac{2\pi \cdot a \cdot \cos(\phi)}{\lambda} = 3.8$, which is depicted by the left vertical dashed line in Figure S3e. Waves with wavenumbers, n, smaller and equal to the separation number rounded to the integer part, $n \leq \lfloor n_{syno} \rfloor = 3$, are associated to larger planetary scale. The wave of the separation number rounded to the least integer, $n = \lceil n_{syno} \rceil = 4$, is separated among the planetary and synoptic scale, by weight of the decimal digit of the separation number. Hence, the planetary scale gets attributed the fraction $n_{syno} - \lfloor n_{syno} \rfloor = 0.8$ of this wave and the remaining fraction, $\lceil n_{syno} \rceil - n_{syno} = 0.2$, is attributed to the synoptic scale. Waves with wavenumbers larger than the separation number rounded to the least integer, $n > \lceil n_{syno} \rceil = 4$, are associated to the synoptic scale.

If no weighting was applied at wave $\lceil n_{syno} \rceil = 4$, the method would produce discontinuous values in the scale-separated energy transport where $\lceil n_s \rceil$ is different for adjacent latitudes (see Fig. S2a). This method ensures a continuous transition across latitudes.

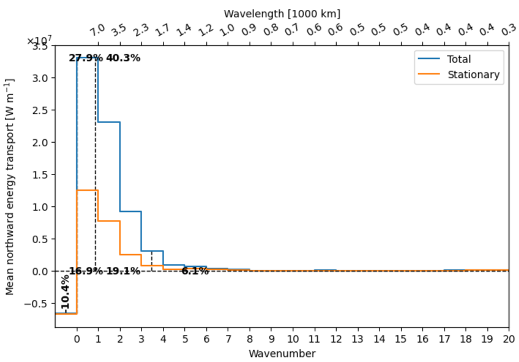

(a) 80°N

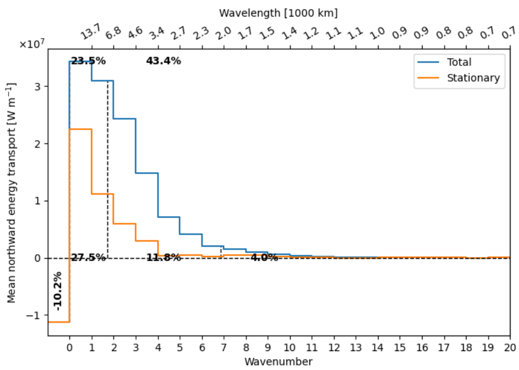

(b) 70°N

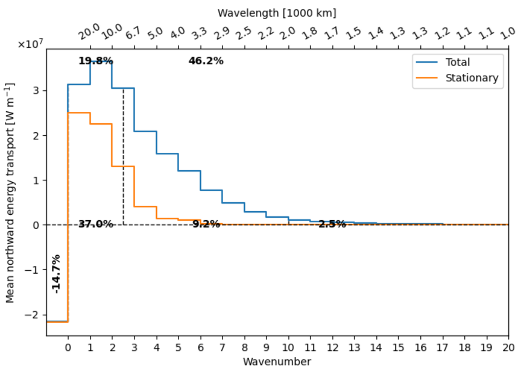

(c) 60°N

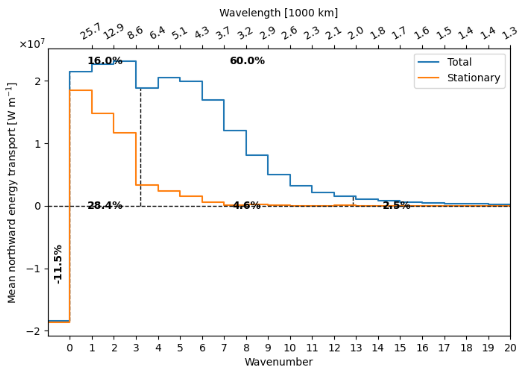

(d) 50°N

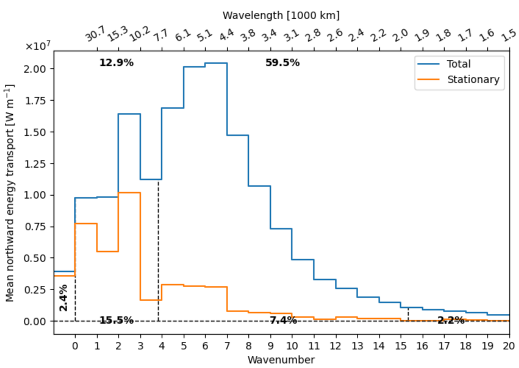

(e) 40°N

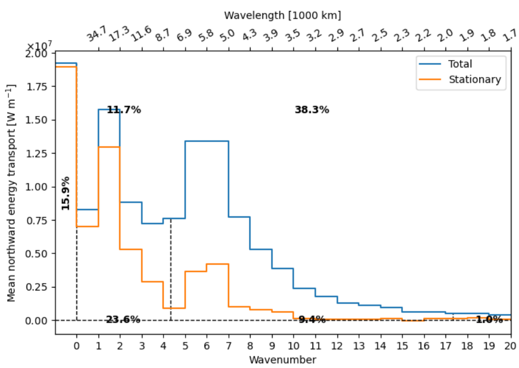

(f) 30°N

Figure S3: Total energy transport across different latitudes from ERA5 decomposed by wavenumber as total (blue) and stationary (orange) contribution. The corresponding wavelengths to the wavenumbers are displayed on top of the plots. Vertical dashed lines separate the different spatial scales. The first at wave 0 between the meridional overturning circulation and planetary waves, the second between the latter and synoptic waves, and the last towards meso-scale waves. Numbers in percentage denote fraction of transport attributed to the different transport components. The rotated number is the meridional overturning circulation, numbers along the x-axis are the stationary contributions, and numbers close to the top of the figure are the transient (total - stationary) contributions, the right-most number is the total meso-scale transport.

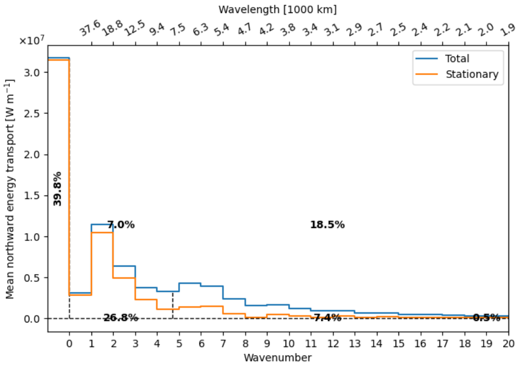

(g) 20°N

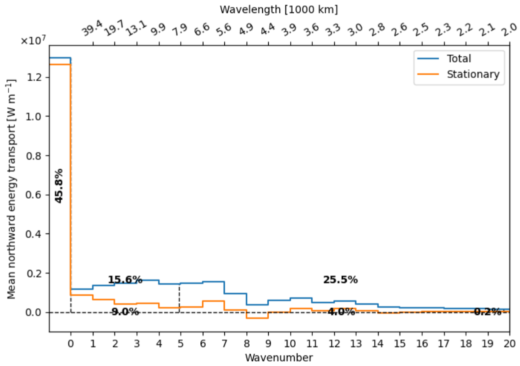

(h) 10°N

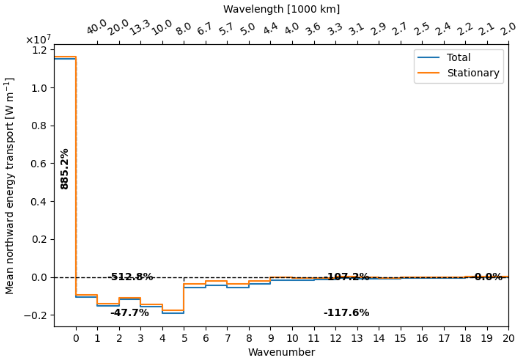

(i) 0°N

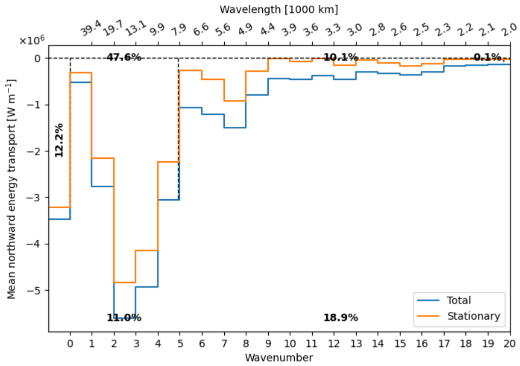

(j) 10°S

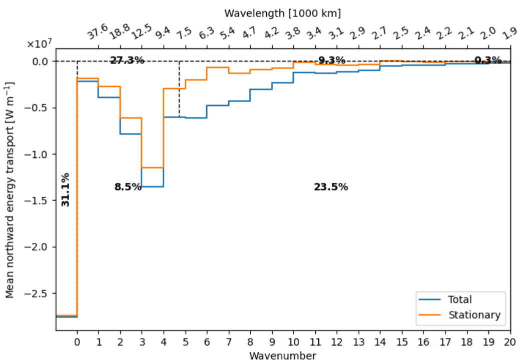

(k) 20°S

Figure S3: Continued

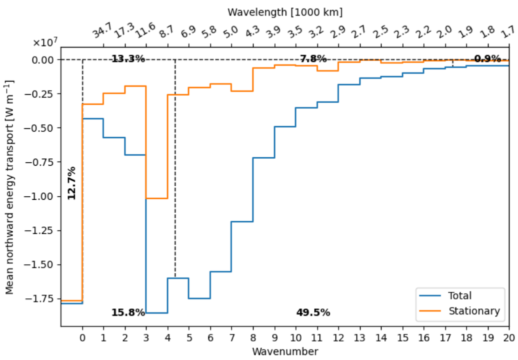

(l) 30°S

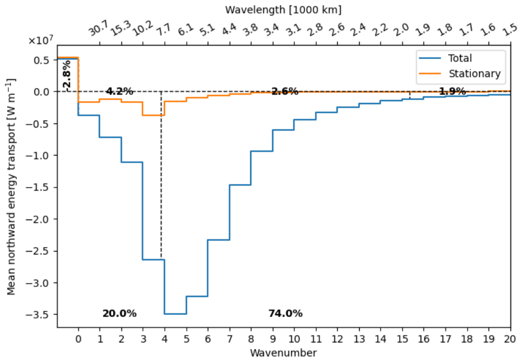

(m) 40°S

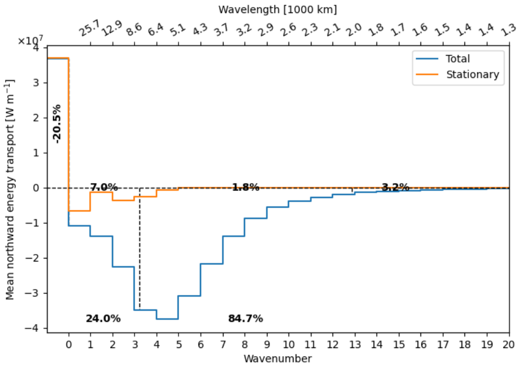

(n) 50°S

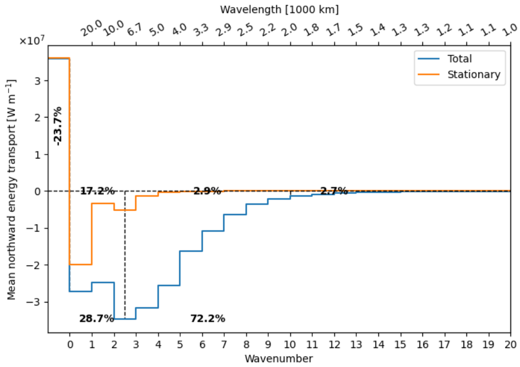

(o) 60°S

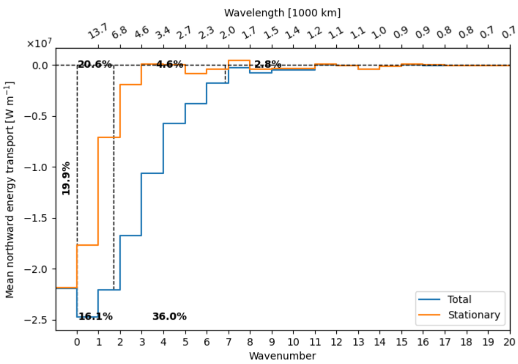

(p) 70°S

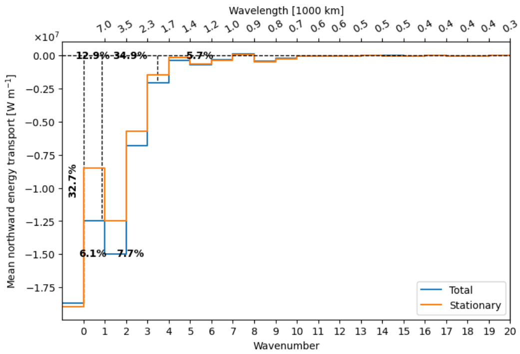

(q) 80°S

Figure S3: Continued

4 Separation of total energy versus the humidity transport

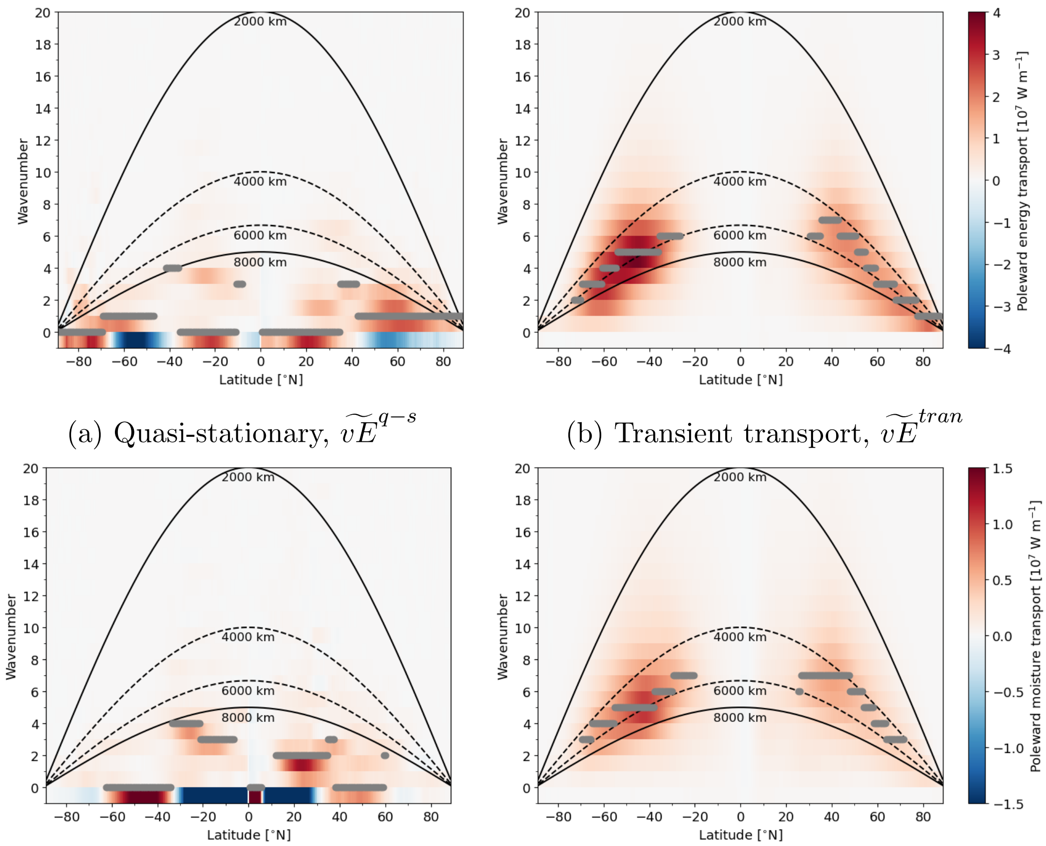

(a) Quasi-stationary, $\widetilde{vE}^{q-s}$

(b) Transient transport, $\widetilde{vE}^{tran}$

(c) Quasi-stationary, $\widetilde{vQ}^{q-s}$

(d) Transient transport, $\widetilde{vQ}^{tran}$

Figure S4: (a,b) Figure 2, (c,d) the same for the moisture transport, being the annual-mean, zonal-mean of the Fourier-decomposed poleward transport of moisture from ERA5 for each latitude. (a,c) Depicts the decomposition of the quasi-stationary and (b,d) of the transient energy transport. The wavenumbers corresponding to wavelengths of 2000, 4000, 6000, and 8000 km are presented by black curves. The solid black curves at 2000 and 8000 km denote the separation between meso, synoptic and planetary scale. At each latitude the wave of maximal poleward energy transport is denoted in grey, where values are masked if the wave is responsible for less than 5% of the transport at the latitude with maximum transport.

We provide a short interpretation of the dominant quasi-stationary waves for the total energy transport (Fig. S4a). In most of the tropics and sub-tropics, wave 0 advects most energy, consistent with the dominant role of the meridional overturning circulation in this region. An exception is the band around 10° S, where wave 3 is transporting most of the energy, which can be explained by quasi-stationary monsoon systems in the Walker circulation of the equatorial Southern Hemisphere with

high pressure over the three ocean basins. In the mid-latitudes of both hemispheres, wave 1 transports most energy. Around 40°, waves 3 and 4 are dominant, which is associated to preferred locations of the subtropical highs.
The wavenumber and wavelength of maximum transport is mainly similar for the total transport and the moisture transport (Fig. S4). The most pronounced difference is in the mid-latitudes, where wave 0 is dominant in the moisture transport. This is associated to moisture thermally-direct advection of moisture by the Ferrel cell, whereas the Ferrel cell is thermally-indirect for the total energy transport. However, the summation over the waves included in the planetary or synoptic band is providing a larger contribution to the moisture transport than the Ferrel cell (Fig. 4b).

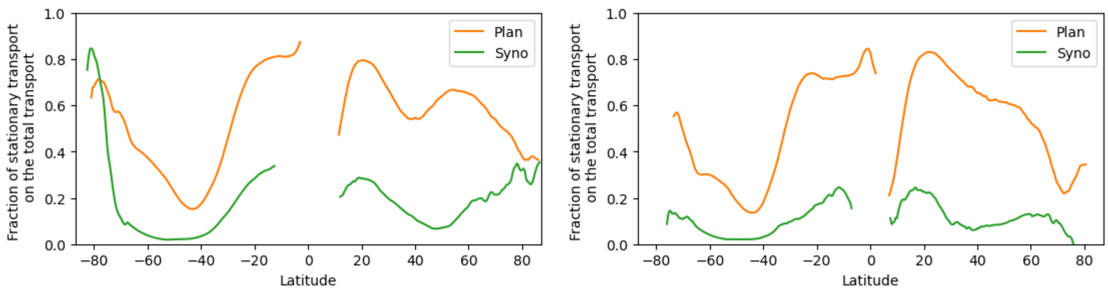

(a) $\widetilde{vE}$ (b) $\widetilde{vQ}$

Figure S5: (a) Fig. 3, (b) the same for the moisture transport. The fraction of the stationary on the total moisture transport of the two major wave components in ERA5.

The fraction of stationary eddies within the planetary and synoptic waves is similar for the total transport and the moisture transport (Fig. S5).

5 Different separations between planetary and synoptic scale

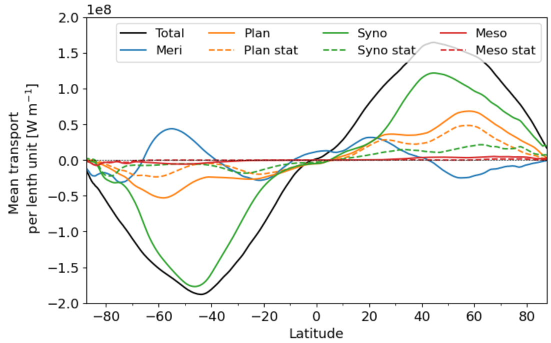

(a) 10000 km

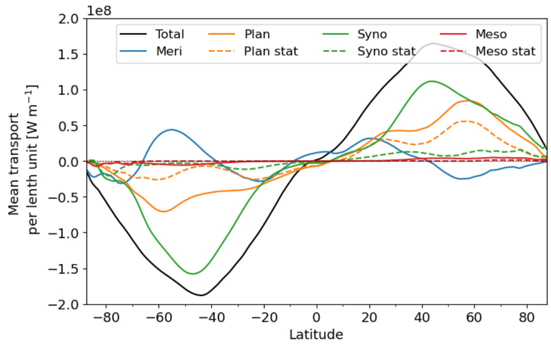

(b) 8000 km

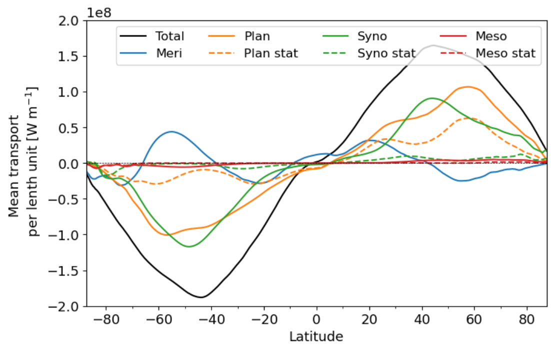

(c) 6000 km

Figure S6: Sensitivity of the partition of the total energy transport into scales at different wavelengths of separation between the planetary and synoptic scale of (a) 10,000 km, (b) 8,000 km as utilised in the study, and (c) 6,000 km. The figure depicts the annual-mean, zonal-mean meridional atmospheric energy transport from ERA5 for the years 1979 - 2018 (black). The energy transport is divided into the zonally symmetric meridional overturning circulation (blue) and wave components at the planetary (orange), synoptic (green), and mesoscale (red, $<$ 2000 km). The (quasi-)stationary contribution on a monthly scale of the different wave components is depicted in dashed lines.

In order to test the sensitivity of the scale separated energy transport for different values of the wavelength used for separation, the latter is varied (Fig. S6). Of course, more (less) transport is associated to the synoptic scale when separation wavelength is increased (decreased), as the wavelength band between 6,000 and 10,000 km comprises a considerable amount of the energy transport (see also Fig. S3). This means that the strength of the synoptic as compared to the planetary component is influenced. However, the important features of planetary and synoptic waves are similar, such as the maximum in the synoptic transport around 45°latitude, the maximum of the planetary around 60°latitude, almost symmetrical structures in both hemispheres, and similar seasonal behaviour (not shown).

6 Spring and autumn energy transport

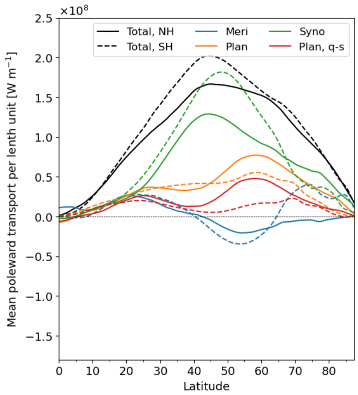

(a) $\widetilde{vE}$; autumn

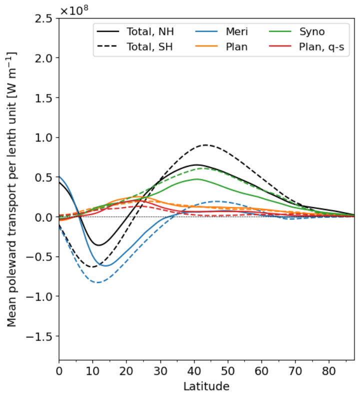

(b) $\widetilde{vQ}$; autumn

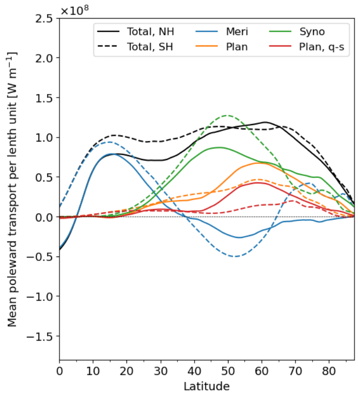

(c) $\widetilde{vD}$; autumn

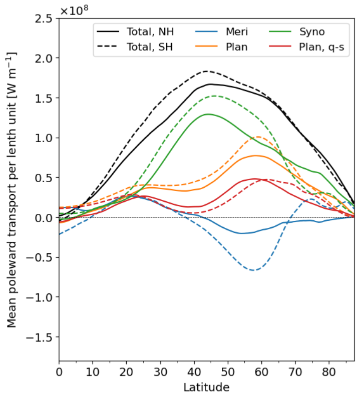

(d) $\widetilde{vE}$; spring

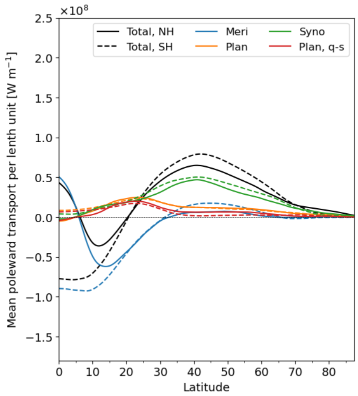

(e) $\widetilde{vQ}$; spring

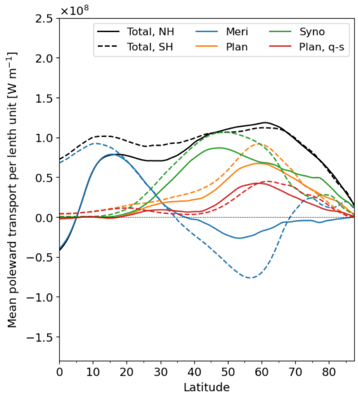

(f) $\widetilde{vD}$; spring

Figure S7: As Figure 4, but for the seasonal-mean transport of (a,b) December to February (DJF), and (c,d) June to August (JJA).

References

Rune G Graversen and Mattias Burtu. Arctic amplification enhanced by latent energy transport of atmospheric planetary waves. *Quarterly Journal of the Royal Meteorological Society*, 142(698):2046–2054, 2016.